· Article ·
doi: 10.13679/j.advps.2016.4.00264

Advances in Polar Science
December 2016 Vol. 27 No. 4: 264-271

Estimating sea ice albedo feedback in a regional climate modeling sensitivity experiment

LIAN Yu[1*], LI Yaosun[1] & CAI Lei[2]

[1] Yunnan Meteorological Observatory, Kunming 650034, China;

[2] International Arctic Research Center, University of Alaska Fairbanks, AK 99775, USA

Received 10 June 2016; accepted 2 December 2016

Abstract Surface albedo feedback (SAF), or sea ice albedo feedback over the Arctic Ocean, has an important effect on the Arctic climate, even though it is not the leading contributor to polar amplification. Previous model-based studies on SAF have primarily used global climate models to exploit their global coverage and favorable configurations. This study verified the capability of using regional climate models (RCMs) to investigate SAF by designing a sensitivity experiment in terms of sea ice coverage. This study modeled two control cases of the years 1980 and 2012, as well as two sensitivity cases performed by switching the sea ice coverages in the control cases. The results proved the Weather Research and Forecast model capable of separating and quantifying the respective contributions of the atmosphere and the surface albedo to the surface radiation budget. Supported by the ALL/CLR model, the balanced surface shortwave radiation absorption was used to calculate SAF. The experiments overestimated SAF, largely because of the canceled cloud effect during model initialization. This study highlights a new possibility of designing experiments for studying climatic sensitivity and feedback using RCMs.

Keywords **surface albedo feedback, numerical simulation, sea ice decline**

Citation: Lian Y, Li Y S, Cai L. Estimating sea ice albedo feedback in a regional climate modeling sensitivity experiment. Adv Polar Sci, 2016, 27: 264-271, doi: 10.13679/j.advps.2016.4.00264

1 Introduction

Surface albedo feedback (SAF) defines the climatic process by which more (less) radiative energy is absorbed at the earth surface because of the decrease (increase) of the surface albedo. It is a positive feedback mechanism that has the tendency to increase without any other external interference[1]. Seasonal melting/freezing of ice and snow produces stronger surface albedo variation and feedback in the Arctic than at lower latitudes[2]. Winton[3] quantified this feedback by raising a simple equation:

$$SAF = \frac{\partial S}{\partial \alpha}\frac{\partial \alpha}{\partial T} \approx \frac{\Delta S_{\alpha \to \alpha'}}{\Delta T}, \quad (1)$$

in which $\Delta S_{\alpha \to \alpha'}$ represents the top-of-atmosphere (TOA) shortwave radiation flux change due to the albedo change from α to α', and ΔT is the corresponding surface air temperature difference. The unit of SAF is $W \cdot m^{-2} \cdot K^{-1}$.

Polar amplification, which is a phenomenon whereby the surface temperature increase in association with global warming is higher in the Arctic than lower latitudes, has been recognized since the 1960s[4]. Early studies suggested the physical driver of polar amplification was SAF, which resulted from the combination of sea ice loss in the oceans and longer snowmelt seasons on land that led to a reduction in surface albedo[5]. As understanding of climate dynamics improved and numerical models became more sophisticated, debate about the contribution of SAF to polar amplification intensified. For example, sensitivity experiments with global climate models (GCMs) without surface albedo forcing were also found to produce polar amplification[6]. Pithan and Mauritsen[6] suggested the dominant contribution to polar amplification was temperature feedback, in which more radiation (energy) was emitted back to space from lower latitudes than higher latitudes in response to surface warming. Although SAF is not the main contributor to polar amplification, sea ice decline has played an important role concerning additional warming over the Arctic via excessive heat flux transfer from open-water

* Corresponding author, E-mail: 13465494@qq.com

areas[7]. Since the 1970s, the minimum coverage of Arctic sea ice has declined considerably[8]. Although its importance is controversial, sea ice decline prevents SAF becoming a positive effect on polar amplification[9]. Quantifying the magnitude and variability of SAF due to Arctic sea ice decline could help establish better understanding of Arctic response to global warming.

Most previous model-based SAF studies have used GCMs because of their global coverage and favorable physical parameterizations[10-12], while regional climate models (RCMs) with their higher spatial resolutions have been used primarily for regional climate studies[13]. However, the latest generation GCMs and RCMs share comparable parameterization schemes. Furthermore, RCMs also have potential for performing radiation sensitivity studies, including quantifying SAF. Although SAF is not the leading contributor to polar amplification, it might have other significant regional climatic effects, such as permafrost degradation beneath the Arctic tundra. The potential capability of estimating SAF using an RCM approach offers a new opportunity for exploring and projecting the hydrological and ecological impacts of global warming on a regional basis.

One approach commonly used to estimate SAF using GCMs is to increase the CO_2 concentration (e.g., $2\times CO_2$ or $4\times CO_2$ scenarios). The correspondingly strengthened greenhouse effect generates a longer snow/ice-free season over the Arctic, which is usually inapplicable within an RCM framework. The alternative introduced in this study applied a sensitivity test by changing the surface albedo field, or in this case, by changing the sea ice coverage. The difficulty of this approach is to isolate the radiative flux and surface temperature changes attributable solely to the altered surface albedo. This study verified the capability of an RCM for discovering radiative sensitivity without operating climatic-scale simulations, but by adopting multiple regional sensitivity tests instead. A radiative balance model (ALL/CLR model) for calculating SAF based on GCM experiments was applied to RCM cases with switched sea ice coverages. This allowed the shortwave flux and surface temperature change corresponding to surface albedo variation to be isolated by switching the sea ice coverage between two cases.

2 Data source

2.1 Polar Weather Research and Forecasting model

The Weather Research and Forecasting (WRF) model is a flexible, state-of-the-art atmospheric modeling system that specifically facilitates regional climate modeling[13]. This study used the Polar WRF model version 3.6.1, which is originated from the WRF model with upgrades based on the experience of regional modeling over the polar region by the Polar Meteorology Group of the Byrd Polar and Climate Research Center at Ohio State University[14-15]. Unlike the original WRF model, the Polar WRF model includes optimized parameterization scheme settings and calibrated land-use profiles designed specifically for modeling on both land and ocean over the Arctic[14,16-17].

2.2 ERA-Interim data set

The ERA-Interim data set was chosen to force the Polar WRF model. It is the latest generation of reanalysis data, issued by the European Centre for Medium-Range Weather Forecasts (ECMWF), which provides gridded atmospheric elements globally[18]. As the upgraded version of ERA-40, which is a second generation reanalysis data set covering the years 1957–2002[19], the ERA-Interim data set has overcome some previous data-assimilation problems that caused the accuracies of certain ERA-40 variables to deviate. Of particular concern were variables concerning the hydrological cycle and precipitation, both of which have dominant effects on the quality of WRF runs[18]. Moreover, the ERA-Interim data set has been shown capable of providing better quality gridded climatic variables in high-latitude areas compared with other reanalysis products[20-21].

3 Methodology

3.1 Model initialization

Inspired by the observed declining trend of September Arctic sea ice extent (Figure 1), this study chose the years of 1980 and 2012 as the simulation periods. Sea ice extent data provided, by the National Snow and Ice Data Center[8] (NSIDC), indicate the area of sea ice coverage in 1980 was almost twice that in 2012 for the months of September. This reduction has caused different sea surface albedos over the Beaufort and Chukchi seas. The simulation domain was centered over the area with the greatest annual variability in sea ice extent, incorporating part of the Chukchi Sea and the Beaufort Sea located off the coast of Alaska (Figure 2).

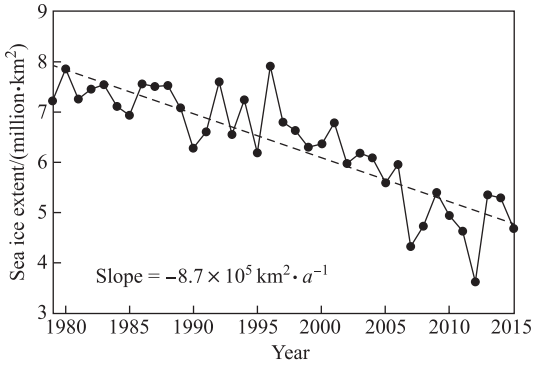

Figure 1 Time series of September sea ice extent of the Northern Hemisphere from 1979 to 2015. Data from the National Snow and Ice Data Center.

The simulation grid had 20-km grid spacing with a total of 89×74 grid points on each of 31 atmospheric layers. Both the initial and the boundary conditions (lateral atmospheric boundaries and surface boundary), including the prescribed

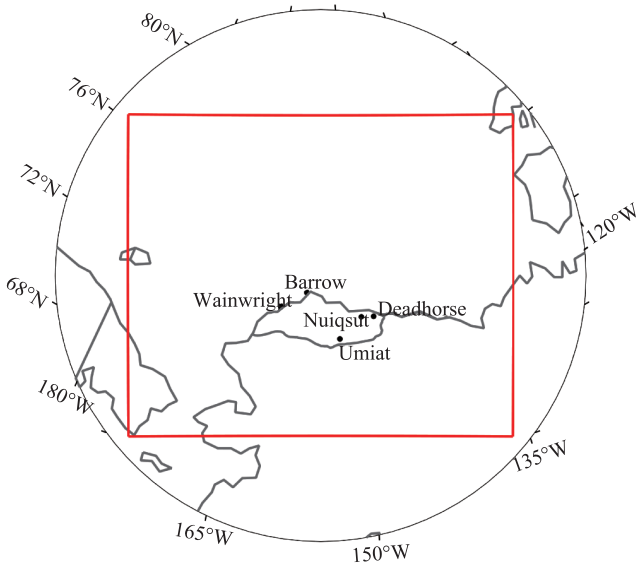

Figure 2 Simulation domain (red box).

sea ice, were imported from the ERA-Interim data set. The boundary conditions were updated at 6-h intervals, except for sea ice coverage, which was updated daily. Importantly, the cloud effect was turned off to prevent cloud layers absorbing, scattering, or reflecting radiation fluxes from the TOA or the surface. The pros and cons of the model setup are discussed in detail in the next section.

Based on the ALL/CLR model algorithm, four sensitivity cases were designed in this study (Table 1): the original simulation of 1980 (1980), original simulation of 2012 (2012), 1980 simulation with 2012 sea ice condition (1980'), and 2012 simulation with 1980 sea ice condition (2012'). The temperature at which seawater freezes into sea ice in the WRF model is 271.35 K; thus, these experiments revised the SST field accordingly based on this logic. This eliminates the case where sea ice exists over warm water (i.e., above freezing point), preventing the model run from crashing. Not switching the SST field along with the sea ice field prevented unrealistic near-surface atmospheric heating by an overly warm sea surface. Because of the relatively cold environment of the Arctic, experimental runs revealed only very small changes of the turbulent heat fluxes caused by the prescribed SST and sea ice, which was beneficial for the research experiments.

Table 1 List of cases modeled in this study

Case name	Temporal range	Atmosphere	Sea ice
1980	1980	1980	1980
2012	2012	2012	2012
1980'	1980	1980	2012
2012'	2012	2012	1980

Multiple parameterization schemes are employed in the WRF model for different physical processes. For microphysical processes, the WRF single-moment 5-class scheme was chosen[22]. The Noah land surface scheme[23] was responsible for land surface processes, and the Yonsei University scheme[24] was used to parameterize planetary boundary layer dynamics. The simulations used the Kain–Fritsch convective parameterization[25]. As the most important schemes for this particular research, the Rapid Radiation Transfer Model[26] (RRTM) and Dudhia scheme[27] were used for longwave and shortwave radiation, respectively. Other than the five trace gases (CO_2, CH_4, O_3, N_2O, and CFCs) included with a constant mixing ratio as part of the atmosphere in the scheme, the RRTM parameterizes the water vapor effect on the radiative balance equation in a relatively simple manner. This made it easy to estimate the radiative absorption effect by water vapor in this study.

3.2 ALL/CLR model

The ALL/CLR model was developed by Winton, based on his 4-parameter model that quantifies SAF, as a simplification that requires one less variable to calculate the surface radiation budget without introducing unacceptable errors[28].

The ALL/CLR model simplifies SAF evaluation by calculating the surface shortwave absorption change due to the albedo change in a smart way[28]. In the original ALL/CLR model, surface shortwave absorption is obtained using the following equation:

$$S_B(S_{B\downarrow},S_{B\uparrow},\alpha_\uparrow,\alpha_s)=S_{B\downarrow}(1-\alpha_s)\times\left(1-\frac{\alpha_\uparrow S_{B\uparrow}}{S_{B\downarrow}}\right)/(1-\alpha_\uparrow\alpha_s), \quad (2)$$

where S_B stands for the surface shortwave absorption, which is equivalent to the downward shortwave flux ($S_{B\downarrow}$) subtracted from the upward shortwave flux ($S_{B\uparrow}$) at the surface, and α_s and $\alpha_\uparrow$ represent the surface albedo and the TOA albedo, respectively. As the cloud effect was turned off in the WRF model, the part following the multiplication sign is approximately equal to 1. Thus, by neglecting it, surface shortwave absorption can be regarded as that part of the downward shortwave radiation that is not reflected after hitting the surface, i.e., the term before the multiplication sign in the above equation. Then, the surface shortwave absorption variation resulting solely from surface albedo change can be calculated using the following equation:

$$\Delta S_{\alpha\to\alpha'}=\frac{S_B(S_{B\downarrow},S_{B\uparrow},\alpha_\uparrow,\alpha_{s'})-S_B(S_{B\downarrow},S_{B\uparrow},\alpha_\uparrow,\alpha_s)+S_B(S_{B\downarrow},S_{B\uparrow},\alpha_\uparrow,\alpha_{s'})-S_B(S_{B\downarrow},S_{B\uparrow},\alpha_\uparrow,\alpha_s)}{2}. \quad (3)$$

Winton[3] proved that the shortwave flux variation due to albedo change at the TOA is approximately equal to the change at the surface. This can simplify the computation because the former can be replaced by the latter, not to mention that the difference in this study was even smaller because the cloud effect was turned off. This set of equations offers the possibility of isolating the changes in total radiation flux attributable to atmospheric and surface variations. To quantify the radiation flux change attributable only to surface optical properties, the ALL/CLR model

averages the subtraction between the same surface optical property but different atmospheric backgrounds, isolating the surface contribution to radiation change and filtering out the atmospheric component.

As the SST field was changed, the surface temperature change was calculated using the 2-m air temperature (T2) instead. Similar to the calculation of $\Delta S_{\alpha\to\alpha'}$, ΔT was obtained using the following equation:

$$\Delta T = \frac{T(S_{B\downarrow},S_{B\uparrow},\alpha_{\uparrow'},\alpha_s) - T(S_{B\downarrow},S_{B\uparrow},\alpha_{\uparrow},\alpha_s) + T(S_{B\downarrow'},S_{B\uparrow'},\alpha_{\uparrow'},\alpha_s) - T(S_{B\downarrow'},S_{B\uparrow'},\alpha_{\uparrow},\alpha_s)}{2}, \quad (4)$$

which averages the surface temperature differences between different atmospheric backgrounds but with the same surface albedo property. This averaging algorithm in the ALL/CLR model isolates that part of surface temperature change due to surface shortwave absorption change alone (i.e., a function of shortwave flux and surface albedo), which provides the possibility of estimating SAF without climatic temporal-scale simulations.

4 Results

4.1 Overview of control cases

The surface optical conditions in 1980 and 2012 were compared beforehand to illustrate the general pattern of albedo change. There was much less sea ice, measured in terms of grid points, and a lower spatially averaged surface albedo during the melting season in 2012 than in 1980 (Figure 3).

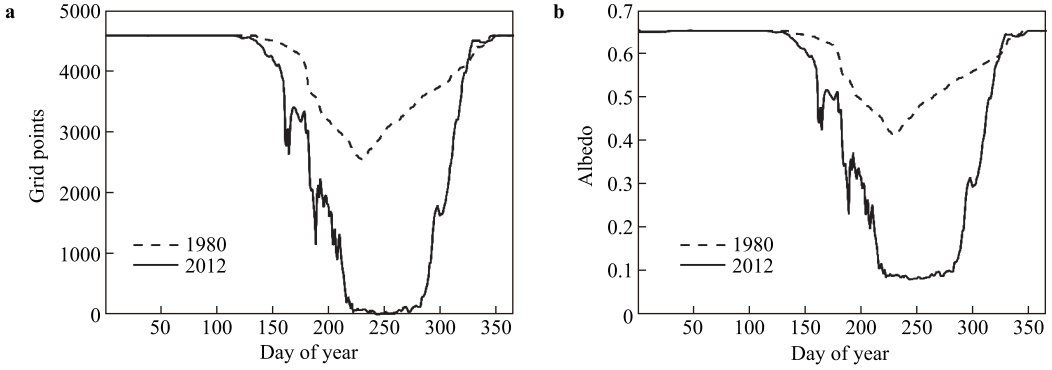

Figure 3 Time series of sea ice coverage (grid points, **a**) in 1980 (dashed line) and in 2012 (solid line) and albedo in 1980 (dashed line) and in 2012 (solid line (**b**)).

The two patterns shown in Figure 3 behave similarly because sea surface albedo depends solely on sea ice coverage in the WRF model. In late August and early September, sea ice coverage within the study area in case 2012 nearly reached zero, which is approximately 60% less than case 1980 at the same time. Correspondingly, the surface albedo of case 2012 was as low as 0.08. Further analysis on how the WRF model deals with sea ice coverage is included in the discussion section.

Spatially, the biggest disparity of the annual mean sea ice extent (annual mean value of variable SEAICE=1 in the WRF model output) between the two cases was found over the southern Beaufort Sea, off the coast of the eastern Alaskan North Slope (Figure 4). The sea ice extent to the north of the Bering Strait varied much less between the two control cases. This indicates a more pronounced surface albedo alteration attributable to the switching of the sea ice coverage in the sensitivity runs.

According to the source code of the RRTM scheme, downward shortwave flux is determined only by the solar zenith angle, latitude, cloud cover, and water vapor, because the trace gas concentrations are fixed in the scheme. In this experiment, the cloud effect was eliminated. This explains why the downward shortwave flux change is correlated negatively with the surface humidity change between the two control cases, with correlation coefficients generally >0.6 (Figure 4). Conversely, the lack of surface humidity disturbance results in almost unchanged shortwave flux at

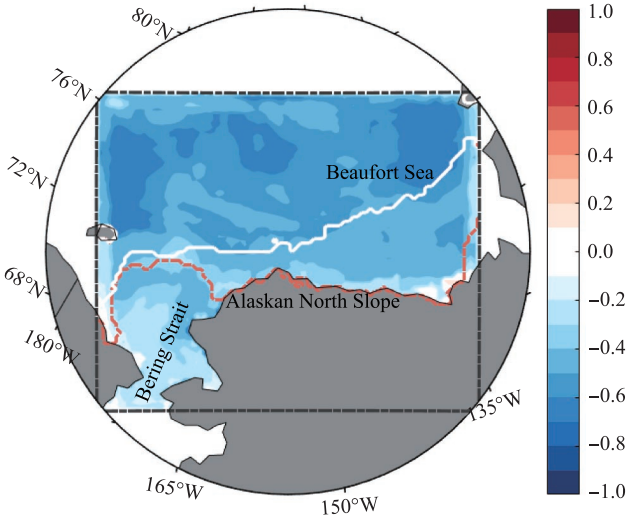

Figure 4 Correlation coefficient between annual mean downward shortwave flux change and surface humidity change (case 1980–case 2012, contours), as well as the annual mean sea ice coverage of case 1980 (white solid line) and case 2012 (red dashed line).

the surface. In this way, surface shortwave absorption is determined solely by surface albedo. Therefore, the difference in sea ice extent between these two cases is sufficiently large to produce a pronounced difference in surface albedo over the ocean, and turning off the cloud effect in this study simplified the analysis of surface shortwave absorption. Additionally, eliminating the cloud effect also removes the reflection by the cloud layer of upward longwave radiation flux emitted from the surface. Thus, the warming effect of the cloud layer in winter, which is important regarding winter air temperature over the Arctic, is negligible.

4.2 Surface radiation budget comparison

Before calculating the surface radiation budget, the five layers of grid points closest to the boundary were trimmed off to filter out boundary biases in the WRF simulations. To examine the reasonability of the sensitivity test design, sea surface shortwave radiation budgets were constructed. If the ALL/CLR model were applicable, the total shortwave radiation absorption changes should be able to be split into two components: one attributable to the atmosphere and the attributable to the land surface. The resulting radiation budgets were found conserved in the experiments. The difference in surface shortwave radiation absorption between the two original cases, 1980 and 2012 (1980→2012), which differ from each other in terms of both the atmosphere and the surface, was about 13.8 W·m^{-2}. This number is equal to the summation via the two pathways of 1980→1980'→2012 and 1980→2012'→2012, which reflect the combined responses of the atmosphere and the surface. This equilibrium of radiation change via these pathways indicates that the WRF's RRTM scheme obeys the fundamental assumption of the ALL/CLR model, which is that the radiation change can be isolated to the contributions attributable to the atmosphere and to the surface. This verifies that the application of the ALL/CLR model in this study was reasonable.

Other than verifying the reasonability of the experimental design, this radiation budget also exhibits the respective contributions from the different elements to the overall surface shortwave absorption (Figure 5). The positive deviations from 1980 to 1980', and from 2012' to 2012, show the consequence of decreasing surface albedo (less sea ice cover) that increases surface shortwave absorption (surface effect). The negative deviations from 1980 to 2012', and from 1980' to 2012, show that less shortwave absorption at the surface resulted from increased atmospheric humidity in 2012 compared with 1980 (atmosphere effect). Comparison of the radiation change due to the atmospheric background with that due to the surface optical property reveals that surface albedo change dominates surface radiation absorption (>60 times higher on average). It proves that atmospheric water vapor plays a minor role in the change of this radiation budget under clear skies, and that the involvement of clouds would naturally increase the atmosphere effect to surface shortwave absorption.

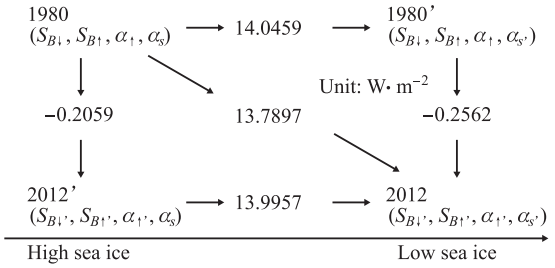

Figure 5 Surface radiation budget of the four sensitivity cases. Arrows indicate the pathways from one case to another and the numbers in between show the surface shortwave radiation absorption difference result from the different case designs (surface and/or atmosphere).

4.3 SAF due to sea ice decline

The radiation budget verified the reasonability of the application of the ALL/CLR model in the sensitivity tests. The SAF and each element that influences it can then be depicted over the simulation domain. Figure 6 shows the spatial distributions of $\Delta S_{\alpha\rightarrow\alpha'}$, $\Delta\alpha$, ΔT, and SAF. The largest differences in shortwave radiation absorption, surface albedo, and surface temperature are all located over the Beaufort Sea. On average, the surface albedo is reduced by >0.3 (Figure 6b). This drop in surface albedo, due to the replacement of seawater by sea ice, causes a difference of >40 W·m^{-2} in surface shortwave absorption (Figure 6a). The change in shortwave absorption is therefore attributable entirely to albedo change, because the cloud effect was eliminated; thus, shortwave radiation extinction by water vapor was proven negligible in this study.

The surface air temperature over the same area shows an increase of 4–5 K. Multiple studies based on both observations and numerical simulations have discussed how sea ice retreat could heat near-surface air. In early winter, remarkable heat loss from an ice-free sea to the near-surface atmosphere occurs because of the heat capacity of the water and latent heat release[29-31]. Furthermore, the increase of near-surface air temperature is also partly attributable to enhanced downward longwave radiation, which is reflected back to the surface from the enhanced cloud cover over the regions of sea ice retreat. By filtering out the cloud effect, this study established that even without the reflection of longwave radiation from the cloud layer, the near-surface air temperature can increase by a magnitude similar to that stated by Porter et al.[31] In contrast, the differences are small over the Chukchi Sea, especially north of the Bering Strait. This is also the case for the Beaufort Sea off the coast of the eastern part of the Alaskan North Slope, where there is no response or even the opposite response. Consequently, SAF is found highest (>10 W·m^{-2}·K^{-1}) over the Beaufort Sea and it is much smaller near the Alaskan North Slope. However, SAF over the sea surface near the Bering Strait is almost absent (<1 W·m^{-2}·K^{-1}) because of the diminished sea ice coverage changes in that area.

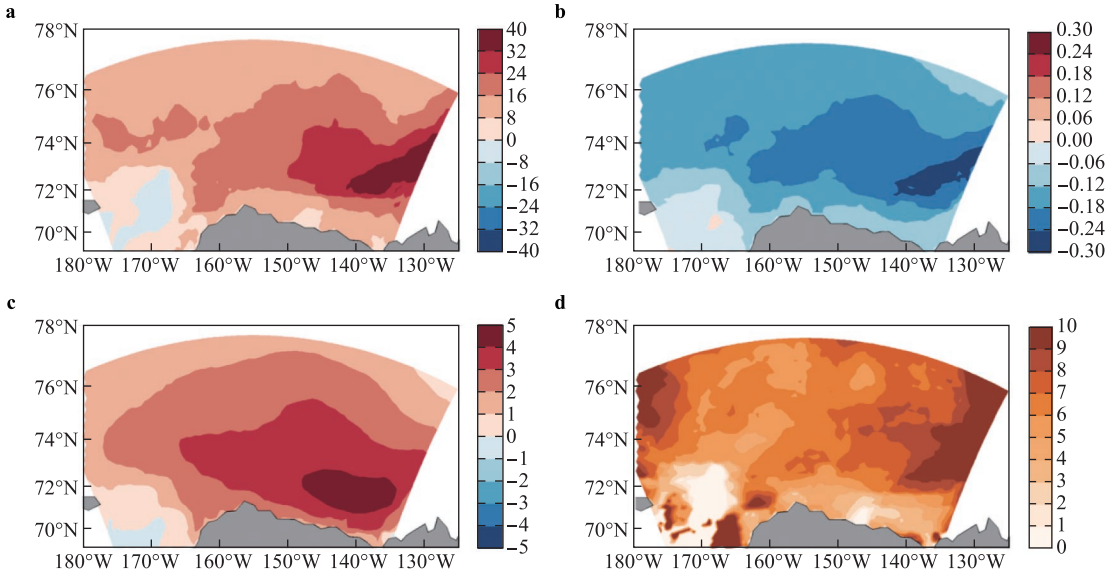

Figure 6 Spatial distributions of annual mean $\Delta S_{\alpha\to\alpha'}$ ($W\cdot m^{-2}$, **a**), $\Delta\alpha$ (**b**), ΔT (K, **c**), and SAF ($W\cdot m^{-2}\cdot K^{-1}$, **d**).

The time series of spatially averaged SAF shows that SAF is nearly nonexistent before April and after October, although the largest difference in sea ice coverage between 1980 and 2012 occurred in October (Figure 7). As a prerequisite of SAF, the lack of solar radiation during winter inhibits SAF considerably. Conversely, SAF comes into effect rapidly in late April, when the sea ice coverage just begins to differ from 1980 to 2012 under the relatively abundant solar radiation flux, and it reaches its maximum around the Summer Solstice.

This WRF-modeled SAF based on a sensitivity test is higher than the SAF magnitude based on reanalysis data sets or GCMs[32-33]. One reason for this is the exclusion of the cloud effect on radiation transfer in the model initialization. A cloud-free atmosphere loses the blocking effect on shortwave radiation, which causes the surface to absorb more shortwave radiation, enhancing SAF. Furthermore, the two years chosen here reflect years in which the sea ice extent was near a maximum and a minimum, rather than the linear trend of nearly four decades. Thus, the opportunity for smoothing the declining trend of sea ice as well as the trend of SAF was lost.

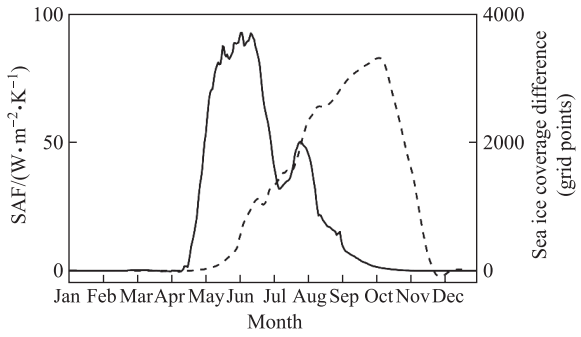

Figure 7 Time series of SAF (solid line) and sea ice coverage difference (1980–2012; dashed line) by grid points.

5 Discussion and conclusions

This research proved that RCMs have the capability of facilitating an examination of SAF without the requirement for long-term simulations by GCMs. The ALL/CLR model enabled a sensitivity experiment approach that saved computational cost. The RRTM scheme was shown suitable for the experiments, providing a conserved surface radiation budget. In addition to the qualified shortwave scheme, some restrictions related to the WRF model (or all the RCMs) remain.

As SST has to be changed in conjunction with sea ice coverage to prevent physical unreality of the surface condition, the algorithm for revising the SST fields needs to be designed carefully to prevent extra moisture being introduced by arbitrarily higher temperatures of the water body. In this case, SST adjustment obeys the criterion for a certain grid, whereby if the switched sea ice covered warm water (SST>271.35 K), the SST value of that grid point was set to 271.35 K; otherwise, it retained its original value. Moreover, the WRF model treats sea ice extent in an approximate manner, i.e., SEAICE=1 for 100% sea ice coverage and SEAICE=0 for open water. This treatment might lead to large biases of the calculated SAF during melting/freezing periods. At specific times when the surface albedo changes from 0.65 to 0.08 (melting) and from 0.08 to 0.65 (freezing), the change is so rapid that the surface temperature does not react at the same pace. This forms outliers (infinite SAFs) in the time series of SAF, which must be removed before further analyses are addressed.

Another source of bias stems from leads within the sea ice pack. The WRF model treats sea ice coverage by grids, and the sea ice parameters are uniform within each grid, which neglects the presence of leads (open water) between areas of ice cover. The Polar WRF model optimizes ice albedo

in terms of sea ice by changing the ice albedo from 0.8 (which is the parameter in the original WRF model) to 0.65; thus, parameterizing an unchanged lead to an ice cover ratio[13]. It is easy to imply that leads within ice packs will expand as the sea ice declines under a warming climate, creating a higher ratio of leads to ice cover and an overall lower surface albedo. In this way, the sea ice albedo might be set to a lower level than 0.65 if applying the WRF simulations forced by future scenarios, such as the dynamical downscaling of GCM projections, assuming that a higher percentage of leads by area will exist in future sea ice cover.

In conclusion, the shortwave parameterization scheme gives the WRF model the capability of calculating SAF, although some limitations remain. The Polar WRF model is capable of capturing the response of sea ice retreat in several respects. The surface shortwave absorption increase is attributable entirely to surface albedo change, and the dominant contributor to the increase of surface air temperature is sea ice retreat.

The purpose of this research was to propose an experimental design rather than to study SAF over this simulation domain in detail. However, this research has built a platform that enables the use of RCMs to address SAF with manageable computational overheads. By involving the cloud effect in future experiments, it will be possible to quantify the influence of cloud cover on SAF. Future improvements include both the application of this approach to long-term downscaled RCM simulations with clouds and the comparison of historical and projected SAFs to those simulated by GCM forcing.

Acknowledgements We thank Xin Rong for his technical support on the WRF simulations and for debugging scripts for SAF analysis. We also thank the two anonymous reviewers for their constructive comments and suggestions, which helped us improve this paper considerably.

References

1 Deser C, Walsh J E, Timlin M S. Arctic sea ice variability in the context of recent atmospheric circulation trends. J Climate, 2000, 13(3): 617–633

2 Cubasch U, Meehl G A, Boer G J, et al. Projections of future climate change//Houghton J T, Ding Y, Griggs D J, et al. Climate Change 2001: the Scientific Basis: Contribution of Working Group I to the third Assessment Report of the Intergovernmental Panel on Climate Change. Cambridge: Cambridge University Press, 2001: 526–582

3 Winton M. Surface albedo feedback estimates for the AR4 climate models. J Climate, 2006, 19(3): 359–365

4 Serreze M C, Barry R G. Processes and impacts of Arctic amplification: a research synthesis. Glob Planet Change, 2011, 77(1–2): 85–96

5 Budyko M I. The effect of solar radiation variations on the climate of the Earth. Tellus, 1969, 21(5): 611–619

6 Pithan F, Mauritsen T. Arctic amplification dominated by temperature feedbacks in contemporary climate models. Nat Geosci, 2014, 7(3): 181–184

7 Serreze M C, Barrett A P, Stroeve J C, et al. The emergence of surface-based Arctic amplification. Cryosphere, 2009, 3(1): 11–19

8 Walsh J E, Fetterer F, Stewart J S, et al.A database for depicting Arctic sea ice variations back to 1850. Geograph Rev, 2017, 107(1): 89–107

9 Winton M. Amplified Arctic climate change: what does surface albedo feedback have to do with it? Geophys Res Lett, 2006, 33(3), doi: 10.1029/2005GL025244

10 Hall A. The role of surface albedo feedback in climate. J Climate, 2004, 17(7): 1550–1568

11 Ingram W J, Wilson C A, Mitchell J F B. Modeling climate change: an assessment of sea ice and surface albedo feedbacks. J Geophys Res, 1989, 94(D6): 8609–8622

12 Qu X, Hall A. What controls the strength of snow-albedo feedback? J Climate, 2007, 20(15): 3971–3981

13 Skamarock W C, Klemp P, Dudhia J,et al. A description of the advanced research WRF version 3.NCAR/TN-475+STR. Boulder, CO: National Center for Atmospheric Research, 2008

14 Hines K M, Bromwich D H, Barlage M, et al. Arctic land simulations with Polar WRF//Preprints, 10th Conf. Polar Meteorology and Oceanography.Long Beach, CA:American Meteorological Society, 2009: 17–21

15 Hines K M, Bromwich D H, Bai L S, et al.Development and testing of polar WRF. Part III: Arctic land. J Climate, 2011, 24(1): 26–48

16 Wilson A B, Bromwich D H, Hines K M. Evaluation of Polar WRF forecasts on the Arctic System Reanalysis Domain: surface and upper air analysis. J Geophys Res, 2011, 116(D11), doi: 10.1029/2010JD015013

17 Wilson A B, Bromwich D H, Hines K M. Evaluation of Polar WRF forecasts on the Arctic System Reanalysis Domain: 2. Atmospheric hydrologic cycle. J Geophys Res, 2012, 117(D4), doi: 10.1029/2011JD016765

18 Dee D P, Uppala S M, Simmons A J, et al. The ERA-Interim reanalysis: configuration and performance of the data assimilation system. Quart J Roy Meteor Soc, 2011, 137(656): 553–597

19 Uppala S M, KÅllberg P W, Simmons A J, et al. The ERA-40 re-analysis. Quart J Roy Meteor Soc, 2005, 131(612): 2961–3012

20 Jakobson E, Vihma T, Palo T, et al. Validation of atmospheric reanalyses over the central Arctic Ocean. Geophys Res Lett, 2012, 39(10), doi: 10.1029/2012GL051591

21 Lindsay R, Wensnahan M, Schweiger A, et al. Evaluation of seven different atmospheric reanalysis products in the Arctic. J Climate, 2014, 27(7): 2588–2606

22 Hong S Y, Juang H M H, Zhao Q Y. Implementation of prognostic cloud scheme for a regional spectral model. Mon Wea Rev, 1998, 126(10): 2621–2639

23 Noilhan J, Planton S. A simple parameterization of land surface processes for meteorological models. Mon Wea Rev, 1989, 117(3): 536–549

24 Hong, S Y, Dudhia J. Testing of a new nonlocal boundary layer vertical diffusion scheme in numerical weather prediction applications//20th Conference on Weather Analysis and Forecasting/16th Conference on Numerical Weather Prediction. Seattle, WA, US: American Meteorological Society, 2004

25 Kain J S. The Kain-Fritsch convective parameterization: an update. J Appl Meteor, 2004, 43(1): 170–181

26 Mlawer E J, Taubman S J, Brown P D, et al. Radiative transfer for inhomogeneous atmospheres: RRTM, a validated correlated-k model for the longwave. J Geophys Res, 1997, 102(D14): 16663–16682

27 Dudhia J. A multi-layer soil temperature model for MM5//Preprints, SixthAnnual PSU/NCAR Mesoscale Model Users' Workshop. Boulder, CO, 1996: 22–24

28 Winton M. Simple optical models for diagnosing surface-atmosphere shortwave interactions. J Climate, 2005, 18(18): 3796–3805

29 Palm S P, Strey S T, Spinhirne J, et al. Influence of Arctic sea ice

extent on polar cloud fraction and vertical structure and implications for regional climate. J Geophys Res, 2010, 115(D21), doi: 10.1029/2010JD013900

30 Porter D F, Cassano J J, Serreze M C. Analysis of the Arctic atmospheric energy budget in WRF: a comparison with reanalyses and satellite observations. J Geophys Res, 2011, 116(D22), doi: 10.1029/2011JD016622

31 Porter D F, Cassano J J, Serreze M C. Local and large-scale atmospheric responses to reduced Arctic sea ice and ocean warming in the WRF model. J Geophys Res, 2012, 117(D11), doi: 10.1029/2011JD016969

32 Soden B J, Held I M, Colman R, et al. Quantifying climate feedbacks using radiative kernels. J Climate, 2008, 21(14): 3504–3520

33 Flanner M G, Shell K M, Barlage M, et al. Radiative forcing and albedo feedback from the Northern Hemisphere cryosphere between 1979 and 2008. Nat Geosci, 2011, 4(3): 151–155